Mathematical models for quantifying eruption velocity in degassing pipes based on exsolution of a single gas and simultaneous exsolution of multiple gases

Arturo S. Leon[a,*]

[a]*School of Civil and Construction Engineering, Oregon State University, 101 Kearney Hall, Corvallis, OR 97331-3212, USA*

Abstract

After the limnic eruptions at Nyos and Monoun in the 1980s, degassing pipes were installed to reduce the continuous increase of CO_2 at the bottom of these lakes. The degassing system consists of a vertical pipe from the lake bottom to the surface and a small pump located near the top of the pipe, which raises water in the pipe up to a level where it becomes saturated with gas, which in turn leads to volume expansion and eruption. This paper describes two new mathematical models for predicting eruption velocity in degassing pipes based on exsolution of a single gas and the simultaneous exsolution of multiple gases. The models were applied to the degassing system of lakes Nyos and Monoun, which contain two main gases, namely CO_2 and CH_4. Because the volume proportion of CH_4 is significant only in Lake Monoun, the Lake Nyos test case considered the CO_2 gas only, while as the Lake Monoun test case considered the simultaneous exsolution of CO_2 and CH_4. Good agreement between the results of the models and observed data is found for both test cases. The results for the eruption in Lake Monoun considering the two main gases measured in this lake (CO_2 and CH_4) were found to have a better agreement with the measurements compared to the model results obtained considering the main gas only (CO_2).

Keywords: Degassing, Eruption, Exsolution, Lake eruption, Lake Monoun, Lake Nyos, Limnic eruption

1. Introduction

It has been shown that dissolved gas in a liquid is able to power violent eruptions (e.g., Woods 1995, Zhang 1996, Halbwachs et al. 2004, Zhang and Kling 2006, Issa et al. 2014). Two types of gas-driven eruptions are known in nature, namely volcanic eruptions and lake eruptions. Volcanic eruptions are driven mainly by dissolved H_2O in magma at high temperatures (e.g., Wilson

*Corresponding author
Email address: arturo.leon@oregonstate.edu (Arturo S. Leon)

et al. 1980). Lake eruptions are driven mainly by exsolution of CO_2 from water at relatively low temperatures (Sigurdsson et al. 1987). The focus of this paper is on degassing pipes that are being used to reduce the probability of lake eruptions and hence our discussion is limited to this type of eruption. There are at least two known occurrences of lake eruptions, one in August of 1984 (Lake Monoun) and the other in August of 1986 (Lake Nyos), both in Cameroon, Africa. The eruption of Lake Monoun killed about 37 people, and the eruption of Lake Nyos killed about 1700 people up to 26 km away from the lake (Zhang and Kling 2006).

During lake eruptions, large amounts of pressurized carbon dioxide, which were previously dissolved in the lower layers of the lakes, are released to the atmosphere (e.g., Sigurdsson et al. 1987, Halbwachs et al. 2004). These eruptions could be triggered by any external disturbance or intrinsic instability of the lake, which could destabilize the density stratification of the lakes' water column (CO_2-laden water is denser than pure water), and hence release suffocating carbon dioxide (e.g., Halbwachs et al. 2004).

After the CO_2 eruption in Lakes Nyos and Monoun in the 1980s, degassing pipes were installed in Lake Nyos in 2001 and in Lake Monoun in 2003 to reduce the continuous increase of CO_2 at the bottom of these lakes (Kusakabe et al. 2000, Halbwachs et al. 2004, Kling et al. 2005). The degassing system consists of a vertical pipe from the lake bottom to the surface (Halbwachs et al. 2004). A small pump located near the top of the pipe, raises the water in the pipe. As the water rises, the pressure decreases as a result both of the work done against gravity and pipe wall friction. The loss of pressure reduces the solubility of the dissolved gas in the moving liquid causing the formation of bubbles or gas exsolution. The exsolved gas causes rapid volume expansion, which accelerates the gas-liquid mixture upwards (foamy water), which in turn causes more gas exsolution due to the continued decompression. The foamy water is more or less a homogenous flow. Once the homogeneous foamy water breaks the water surface, an eruption is produced. Various photographes of these eruptions can be found in Halbwachs et al. (2004).

The volume expansion and eruption processes were verified in the laboratory (e.g., Zhang 1997, Zhang 1998). In one of these experiments, water with high dissolved content of CO_2 in a test cell was suddenly decompressed, leading to CO_2 supersaturation, bubble nucleation and growth, volume expansion, and eruption (Zhang 1997, Zhang 1998). These experiments showed that bubble nucleation is very fast, with a typical incubation time of a couple of milliseconds. The rapid bubble nucleation and bubble growth rates in the experiments may be used to argue that there is quasi-equilibrium between gas phase and liquid phase during geysering (e.g., Zhang and Kling 2006).

Besides volcanic and lake eruptions, gas exsolution may also play a role in geysers occurring in stormwater and combined sewer systems. These systems may contain a mixture of toxic and non-toxic gases that can be present at varying levels depending upon the source (Hutter 1993). The gases present in sewers may include ammonia (NH_3), hydrochloric acid (HCl), hydrogen sulfide (H_2S), methane (CH_4), carbon dioxide (CO_2), carbon monoxide (CO), sulfur

dioxide (SO_2) and chlorine (Cl_2) (Viana et al. 2007, Hutter 1993). For instance, ammonia, which is widely used in fertilizers, may be present in large amounts in stormwater and combined sewer systems. Some of the gases, such as ammonia, are easily absorbed in water. Ledig (1924) has shown that ammonia is absorbed in water at least 100 times faster than carbon dioxide. In most cases, it is likely that dissolved gases are below saturation, however they can be exsolved when the bottom water moves upward to the point where dissolved gas pressure exceeds local hydrostatic pressure.

This paper presents two mathematical models for predicting eruption velocity in degassing pipes based on exsolution of a single gas and the simultaneous exsolution of multiple gases. This paper is divided as follows. First, a mathematical model for quantifying eruption velocity in a degassing pipe based on exsolution of a single gas is presented. Second, the aforementioned model is extended for quantifying eruption velocity in a degassing pipe based on simultaneous exsolution of multiple gases. Third, the two models are applied to the degassing system of lakes Nyos and Monoun. Finally, the key results are summarized in the conclusion.

2. Mathematical model for quantifying eruption velocity in a degassing pipe based on exsolution of a single gas

The assumptions of this model are listed below:

- The bubbly two-phase flow in the vertical pipe is treated as a single-phase equivalent mixed flow.
- The liquid is assumed to be water with constant density (e.g., independent of pressure).
- The decompression process is assumed to be isothermal. This is justified because the decrease in temperature due to gas exsolution and bubble expansion is small, which is mainly due to the high heat capacity ratio of water (e.g., Zhang and Kling 2006).
- There is exsolution of only one gas (e.g., CO_2). The second model addresses simultaneous exsolution of multiple gases.
- The gas is ideal, which is somewhat reasonable at low pressures.

The compressible Navier-Stokes equations for the vertical direction (z) assuming a one-dimensional flow can be written as (Shapiro 1954)

$$\frac{\partial \rho}{\partial t} + \frac{\partial (\rho w)}{\partial z} = 0 \tag{1}$$

$$\frac{\partial w}{\partial t} + \frac{1}{\rho}\frac{\partial p}{\partial z} + w\frac{\partial w}{\partial z} = -g - \frac{f}{2D}w^2 \tag{2}$$

where t is time, p is pressure, ρ is the density of the gas-liquid mixture, g is the gravitational acceleration, z is vertical distance measured from the point where the homogenous gas-liquid mixture starts to accelerate, w is the mixture rise velocity, f is the Darcy-Weisbach friction factor and D is the diameter of the vertical pipe. It is worth to mention that Shapiro (1954) uses the Fanning friction factor instead of the Darcy-Weisbach friction factor. The Darcy-Weisbach friction factor is 4 times larger than the Fanning friction factor. Kim et al. (2015) using experiments with a carbonate mixture flow showed that the friction factor is independent of the fluid type.

Because the degassing is maintained over time, it is reasonable to assume that the degassing is a steady-state flow. Hence, the flow variables (e.g., ρ, p and w) are a function of z only. Thus, the time derivatives in Eqs. (1) and (2) are dropped and the partial derivatives are replaced by total derivatives. With these considerations, Eqs. (1) and (2) can be written as:

$$\rho dw + w d\rho = 0 \tag{3}$$

$$\frac{1}{\rho}\frac{dp}{dz} + w\frac{dw}{dz} = -g - \frac{f}{2D}w^2 \tag{4}$$

Combining Eqs. (3) and (4), the following equation is obtained:

$$(1 - \frac{w^2}{a^2})\frac{1}{\rho}\frac{dp}{dz} = -g - \frac{f}{2D}w^2 \tag{5}$$

where a is the sound speed in the mixture flow given by $\sqrt{dp/d\rho}$. Note in Equation (5) that dp/dz is negative and that both terms in the right side (gravity and friction) are negative. Hence, for Equation (5) to be valid, the following condition needs to be satisfied.

$$w \leq a \tag{6}$$

This means that the maximum velocity of the gas-liquid mixture will be that of its sound speed. An equation for estimating the sound speed of a two-phase mixture is given by Mastin (1995)

$$a = \sqrt{\frac{k_l k_g}{\rho[(1-\phi)k_g + \phi k_l]}} \tag{7}$$

where ϕ is the volume fraction of gas (i.e., ratio of total volume of gas to total volume), k_l and k_g are the bulk modulus of liquid and gas, respectively. Measurements during the degassing of lakes Nyos and Monoun reported gas/water volume ratios ranging from 2.9 to 9 (Halbwachs et al. 2004). The latter indicates that at eruption the values of ϕ would range between 0.24 and 0.76. The bulk modulus of a material, which is the inverse of the compressibility, determines how much the material will compress under a given amount of external pressure. A representative value for the bulk modulus of water is 2.2x10^9 N/m^2 (2200 MPa). The bulk modulus for the gas depends on how the temperature varies

during decompression. As discussed earlier, the temperature is kept more or less constant during the exsolution. For isothermal conditions, the bulk modulus of the gas (k_g) is equal to the gas pressure (Weast 1984). At eruption, the pressure at the top of the degassing pipe will be near atmospheric (0.1 MPa), and hence the term $(1-\phi)k_g$ in Eq. (7) would range between 0.024 and 0.076 MPa and the term ϕk_l would range between 528 and 1672 MPa. Because $(1-\phi)k_g$ is a small fraction of ϕk_l (less than 0.01%), Eq. (7) can be reduced to

$$a \approx \sqrt{\frac{p_g}{\rho\phi}} \tag{8}$$

The density of the gas-liquid mixture is often expressed as $\rho = (1-\phi)\rho_l + \phi\rho_g$ (e.g., Zhang and Kling 2006). As mentioned above, measured values of ϕ ranged between 0.24 and 0.76 (Halbwachs et al. 2004), ρ_l is about 1000 kg/m^3 and ρ_g greatly depends on the pressure and temperature. At eruption, the pressure at the top of the degassing pipe will be near atmospheric. For atmospheric pressure and for temperatures higher than -20°C, the air density will not exceed 1.4 kg/m^3 (`https://en.wikipedia.org/wiki/Density_of_air`). With these considerations, at eruption, the minimum value of $(1-\phi)\rho_l$ would be about 240 kg/m^3 and the maximum value of $\phi\rho_g$ would be 1.06 kg/m^3. Because $\phi\rho_g$ is a small fraction of $(1-\phi)\rho_l$ (less than 0.44%), Eq. (8) can be further simplified to

$$a \approx \sqrt{\frac{p_g}{\phi(1-\phi)\rho_l}} \tag{9}$$

Eq. (9) is the same as that of Zhang and Kling (2006). Following let's estimate the maximum eruption velocity using the governing equations. To integrate Eq. (4), this equation can be rewritten as

$$\int \frac{1}{\rho} dp + \int w dw = -\int g dz - \int \frac{f}{2D} w^2 dz \tag{10}$$

To integrate the first left term of Eq. (10), a relationship between p and ρ is necessary. Because of rapid bubble nucleation and bubble growth, there is quasi-equilibrium between the gas and liquid phases (e.g., Zhang and Kling 2006). Herein, I use the equation of state for a gas-liquid mixture of Zhang (2000) for the condition when there is chemical equilibrium between the liquid and gas phases, which is given by

$$\frac{\rho_l}{\rho} \approx 1 - \delta_o + \delta_o \frac{\rho_l RT}{p_g} + \lambda \frac{p_{g_o}}{p_g} - \lambda \tag{11}$$

where δ_o is the initial mass fraction of the gas, p_o is the initial total gas pressure (e.g., at $z = 0$), R is the gas constant in Jkg^{-1}K^{-1}, T is in K, and λ is the Ostwald solubility coefficient for the gas in water. Table 1 presents the Ostwald solubility coefficient for some gases. This table was extracted from Atomistry (2015).

Table 1. Ostwald's Solubility Coefficient for some gases, extracted from Atomistry (2015)

Gas	10°C	15°C	20°C	25°C
$\mathbf{CH_4}$	0.0418	0.0369	0.0331	0.0301
$\mathbf{CO_2}$	1.194	1.019	0.878	0.759
$\mathbf{Cl_2}$	3.095	2.635	2.26	1.985
$\mathbf{H_2S}$	3.362	2.913	2.554	2.257
$\mathbf{SO_2}$	56.65	47.28	39.37	32.79
HCl	474	456	443	432
$\mathbf{NH_3}$	910	802	710	635

From Table 1, for a temperature of 298.15K (25°C), the solubility coefficient of NH_3, HCl, SO_2, H_2S, Cl_2, CO_2 and CH_4 are 635, 432, 32.79, 2.257, 1.985, 0.759 and 0.0301, respectively. This means that the solubility of NH_3 in water is about 1.5, 19.4, 281.3, 319.9, 836.6 and 21,096.3 times that of HCl, SO_2, H_2S, Cl_2, CO_2 and CH_4, respectively. This indicates that the exsolution of ammonia would be much more significant than those of SO_2, H_2S, Cl_2, CO_2 and CH_4.

Using Eq. (11), the integration of the first term of Eq. (10) is performed between two points along the vertical pipe, e.g., the point at which the gas-liquid mixture starts to accelerate ($z = 0$) and the water surface in the vertical pipe ($z = L$). This gives

$$\int_{p_{g_o}}^{p_{\text{atm}}} \frac{1}{\rho} dp \approx (1 - \delta_o - \lambda)\left(\frac{p_{\text{atm}} - p_{g_o}}{\rho_l}\right) + \left(\delta_o RT + \lambda \frac{p_{g_o}}{\rho_l}\right) \ln\left(\frac{p_{\text{atm}}}{p_{g_o}}\right) \tag{12}$$

The integration of the second and third terms of Eq. (10) do not need explanation. To integrate the last term of Eq. (10), a relationship of f as a function of w and a relationship of w as a function of z are needed.

For estimating the friction factor there are various formulations. For smooth pipes, Joseph and Yang (2010) divided experimental data of friction factors of McKeon et al. (2004) in four subsections, each of which were represented with power laws as follows:

$$\begin{aligned} f &= \frac{64}{Re} \text{ for } 0 < Re < 2900 \\ &= 4.1 \times 10^{-16} Re^4 \text{ for } 2900 < Re < 3050 \\ &= 0.351 Re^{-0.255} \text{ for } 3050 < Re < 240000 \\ &= 0.118 Re^{-0.165} \text{ for } Re > 240000 \end{aligned} \tag{13}$$

For rough pipes, the friction factor is independent of the Reynolds number and f can be calculated using the formula of Von Karman (Schlichting 1979), which was later supported by Nikuradse's experiments:

$$f^{-1/2} = 2 \log_{10}(D/\epsilon) + 1.74 \tag{14}$$

where ϵ is the pipe wall equivalent roughness height. For estimating the variation of velocity as a function of z, the analytical equation obtained for a frictionless degassing pipe is used. For a frictionless degassing pipe ($f = 0$), the integration of Eq. (10) gives the following maximum eruption velocity (w_e)

$$w_e \approx \sqrt{2\left(\left(\delta_o RT + \lambda\frac{p_o}{\rho_l}\right)\ln\left(\frac{p_o}{p_{\text{atm}}}\right) + (1-\delta_o-\lambda)\left(\frac{p_o - p_{\text{atm}}}{\rho_l}\right) - gL\right)} \tag{15}$$

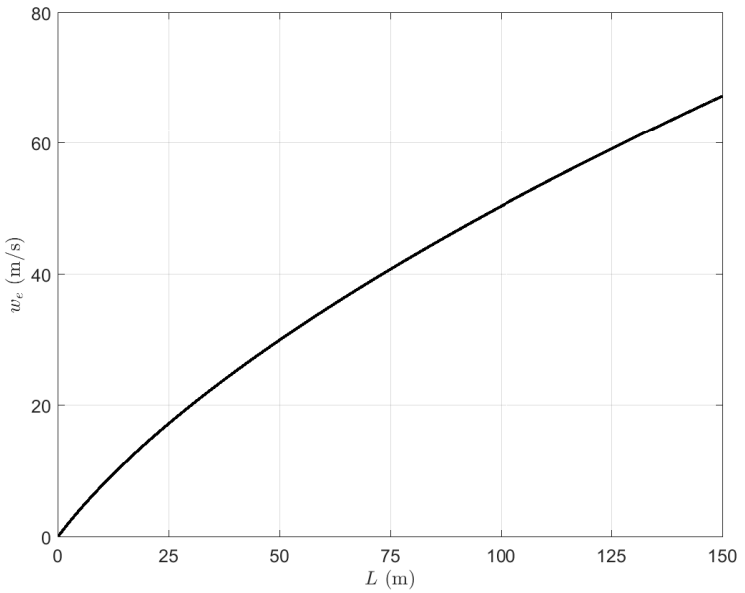

Figure 1. Maximum eruption velocity (w_e) as a function of L for the Lake Nyos test case (Test 1)

where p_{atm} is the atmospheric pressure and L is the distance between the point where the homogenous gas-liquid mixture starts to accelerate and the water surface in the vertical pipe. The plot of w_e in Eq. (15) as a function of L for the Lake Nyos test case (Test 1) is shown in Figure (1). To make a dimensionless plot of the maximum eruption velocity, a reference state is defined (ref). To normalize the plot to values between 0 and 1, the reference values are chosen to be the maximum L (L_{ref}) and its corresponding reference velocity ($w_{e_{ref}}$), which is calculated using Eq. (15). Figure (2) shows the plot of $w_e/w_{e_{ref}}$ versus L/L_{ref} for the Lake Nyos test case, where w_e was calculated using Eq. (15). As can be observed in Figure (2), $w_e/w_{e_{ref}}$ can be represented by a power law of the form

$$\frac{w_e}{w_{e_{ref}}} \approx \left(\frac{L}{L_{ref}}\right)^q \tag{16}$$

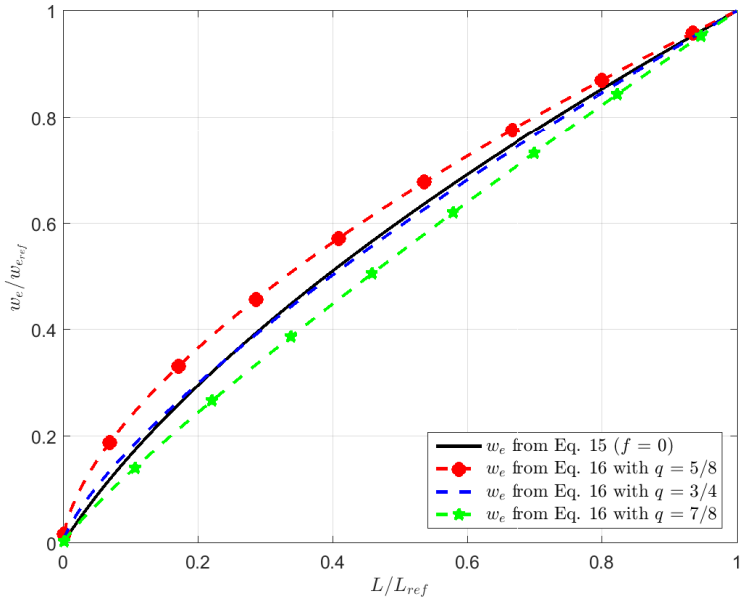

Figure 2. Curve fitting for $w_e/w_{e_{ref}}$ as a function of L/L_{ref}

where q is a constant to be determined. For curve fitting, three values of q were used (5/8, 3/4 and 7/8), the plot of which are shown in Figure (2). According to Figure (2), a value of $q = 3/4$ provides the best fit to $w_e/w_{e_{ref}}$. Similarly, it can be assumed that the ratio of velocity inside the degassing pipe at a given z ($w(z)$) to the maximum eruption velocity (w_e) follows the same power law form as Eq. (16)

$$\frac{w}{w_e} \approx \left(\frac{z}{L}\right)^q \tag{17}$$

To show that the selection of the coefficient doesn't influence much the results, Test case 1 will show the results using three values of q (5/8, 3/4 and 7/8). Note that Eq. (17) is only used to calculate the friction term in Eq. 10 (last right term). When integrating the last right term of Eq. 10 ($\int(f/2D)w^2dz$), a different integration is performed for smooth and rough pipes because the friction factor f is different for each of these cases. For smooth pipes, f is a function of the Reynolds number only as shown in Eq. (13). Even though Eq. (13) shows four formulas of f, each of which is associated to a range of Reynolds numbers, as will be shown below, the fourth formula of f could be applied to the entire range of Reynolds numbers with very good accuracy. The reasons are: (1) after a relatively small distance z, the flow will be in the fourth region, and (2) the term fw^2 in the small distance z is small compared to that of the upper region $(L-z)$ because the squared velocity in the distance z is very small compared to that of the upper region. To show the latter, the plots of fw^2 using

the four relationships of f (Eq. 13) and that using only the fourth relationship are shown in Figure (3). The value of w is obtained from Eq. (17) using $q = 3/4$. As can be observed in Figure (3), the two curves have a very good agreement. Note that the area under the curves is proportional to the integral sought ($\int (f/2D) w^2 dz$). Numerical integration of the two curves in Figure (3) show that the integral of the second curve (4th f in Eq. 13) is 99.99% of the first curve (all four f in Eq. 13), showing that using only the fourth relationship in Eq. (13) for the entire region of Reynold numbers is accurate enough when computing fw^2. For rough pipes, f is only a function of the relative roughness (ϵ/D), however this holds only for high Re. For the same reasons as the case of smooth pipes, for rough pipes, the f value could be applied to the entire range of Reynolds numbers with very good accuracy.

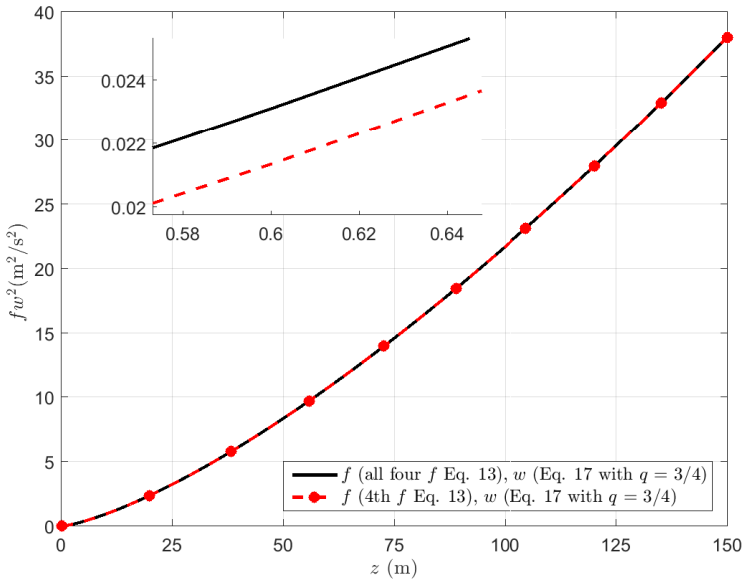

Figure 3. plot of fw^2 in Eq. (10) as a function of z

With the above considerations, for a smooth pipe

$$\int \frac{f}{2D} w^2 dz \approx \frac{0.059}{1 + 1.835q} \frac{L}{D} \left(\frac{D}{\nu}\right)^{-0.165} w_e^{1.835} \tag{18}$$

where ν is the kinematic viscosity. Similarly, for a rough pipe

$$\int \frac{f}{2D} w^2 dz \approx \frac{1}{2(2q+1)} \left(2 \log_{10}\left(\frac{D}{\epsilon}\right) + 1.74\right)^{-2} \frac{L}{D} w_e^2 \tag{19}$$

Collecting terms, the maximum eruption velocity (w_e) for the gas-liquid mixture for a smooth pipe can be obtained by solving for w_e in the following

equation.

$$\frac{w_e^2}{2}+\frac{0.059}{1+1.835q}\frac{L}{D}\left(\frac{D}{\nu}\right)^{-0.165}w_e^{1.835}+gL+(1-\delta_o-\lambda)\left(\frac{p_{\text{atm}}-p_{g_o}}{\rho_l}\right)+\left(\delta_o RT+\lambda\frac{p_{g_o}}{\rho_l}\right)\ln\left(\frac{p_{\text{atm}}}{p_{g_o}}\right)=0 \tag{20}$$

Similarly, the maximum eruption velocity for the gas-liquid mixture for a rough pipe is given by

$$w_e \approx \sqrt{2\left(\frac{\left(\delta_o RT+\lambda\frac{p_o}{\rho_l}\right)\ln\left(\frac{p_o}{p_{\text{atm}}}\right)+(1-\delta_o-\lambda)\left(\frac{p_o-p_{\text{atm}}}{\rho_l}\right)-gL}{1+\frac{1}{2q+1}\frac{fL}{D}}\right)} \tag{21}$$

where f is given by Eq. (14). As mentioned earlier, the maximum eruption velocity cannot exceed the sound speed given by Eq. (9).

3. Mathematical model for quantifying eruption velocity in a degassing pipe based on simultaneous exsolution of multiple gases

In a similar way to the single exsolution model, Eq. (10) can be used to describe the gas-liquid mixture accelerating flow.

To integrate the first left term of Eq. (10), a relationship between p and ρ that considers the simultaneous exsolution of multiple gases is necessary. This equation is found to be (For derivation details see Appendix A)

$$\frac{\rho_l}{\rho}\approx 1+\lambda_i\frac{p_{g_{i,o}}-p_{g_i}}{p_{g_i}} \tag{22}$$

where the subscript i indicates the gas component (e.g., CO_2) and the subscript o indicates the conditions at $z=0$, where the gas is saturated and the gas-liquid mixture starts to accelerate. Also, $p_{g_{i,o}}$ is the partial pressure of gas i at $z=0$, p_{g_i} is the partial pressure of gas i at a given z, and λ_i is the Ostwald solubility coefficient for gas i in water. As is shown in Appendix A, ρ_l/ρ in Eq. (22) can be determined using the information of a single gas (e.g., gas 1).

To calculate the distribution of partial pressures at $z=0$ (e.g., $p_{g_{1,o}}$, $p_{g_{2,o}}$, ...) in Eq. (22), note that exsolution of gases will occur when the total gas pressure (p_o) just exceeds the local pressure. Following, let's consider that data of partial pressures of gases are available at the vertical pipe bottom, and hence the ratio of partial pressure to total pressure for each gas. As mentioned earlier, it is likely that the gases are not saturated at the vertical pipe bottom, however they can become saturated when the water rises along the vertical pipe. Assuming that the aforementioned ratio for each gas at $z=0$ (e.g., at the point where the homogenous gas-liquid mixture starts to accelerate after the total gas pressure just exceeds the local hydrostatic pressure) is the same as that of the pipe bottom, the partial pressure of the gases at $z=0$ (e.g., $p_{g_{1,o}}$, $p_{g_{2,o}}$, ...) will be a fraction of p_o according to the above ratios of partial pressures.

The partial pressures of the gases (e.g., p_{g_i}) are related by (For derivation details see Appendix A)

$$\frac{\lambda_1 p_{g_{1,o}}}{p_{g_1}} - \lambda_1 = \frac{\lambda_i p_{g_{i,o}}}{p_{g_i}} - \lambda_i \ \forall i \text{ from 2 to } n \tag{23}$$

where n is the number of gases. Eq. (23) provides n-1 equations. To determine the partial pressures of the gases at eruption (p_{g_1}, p_{g_2}, ...p_{g_n}), one more equation is needed. This equation is obtained from Dalton's Law which expresses the fact that the total pressure of an ideal gas mixture is the sum of the partial pressures of each individual gas in the mixture. The total pressure at eruption is the atmospheric pressure. Hence

$$p_{atm} = \sum_{i=1}^{n} p_{g_i} \tag{24}$$

Combining Eqs. (23) and (24), p_{g_1} can be solved from the following nonlinear equation

$$p_{g_1} + \sum_{i=2}^{n} \frac{\lambda_i p_{g_{i,o}}}{\lambda_1 \frac{p_{g_{1,o}}}{p_{g_1}} - \lambda_1 + \lambda_i} = p_{atm} \tag{25}$$

For numerical stability reasons when solving Eq. (25), it is recommended to select as gas 1, that with the lowest solubility coefficient. Once p_{g_1} is determined from Eq. (25), p_{g_i} ($\forall$ i from 2 to n) can be determined as follows

$$p_{g_i} = \frac{\lambda_i p_{g_{i,o}}}{\lambda_1 \frac{p_{g_{1,o}}}{p_{g_1}} - \lambda_1 + \lambda_i} \tag{26}$$

Using Eq. (22), the integration of the first term of Eq. (10) gives (For derivation details see Appendix B)

$$\int \frac{1}{\rho} dp = -gL + \frac{1}{\rho_l} \sum_{i=1}^{n} \left[\lambda_i p_{g_{i,o}} \left(1 - \frac{p_{g_i}}{p_{g_{i,o}}} - \ln\left(\frac{p_{g_{i,o}}}{p_{g_i}} \right) \right) \right] \tag{27}$$

The integration of the second, third and fourth terms of Eq. (10) is the same as the first model. Collecting terms, the maximum eruption velocity (w_e) for the gas-liquid mixture for a smooth pipe based on simultaneous exsolution of multiple gases can be obtained by solving for w_e in the following equation.

$$\frac{w_e^2}{2} + \frac{0.059}{1 + 1.835q} \frac{L}{D} \left(\frac{D}{\nu} \right)^{-0.165} w_e^{1.835} + \frac{1}{\rho_l} \sum_{i=1}^{n} \left[\lambda_i p_{g_{i,o}} \left(1 - \frac{p_{g_i}}{p_{g_{i,o}}} - \ln\left(\frac{p_{g_{i,o}}}{p_{g_i}} \right) \right) \right] = 0 \tag{28}$$

Similarly, the maximum eruption velocity (w_e) for the gas-liquid mixture for a

rough pipe based on simultaneous exsolution of multiple gases is given by

$$w_e \approx \sqrt{2\left\{\frac{\frac{1}{\rho_l}\sum_{i=1}^{n}\left[\lambda_i p_{g_{i,o}}\left(\frac{p_{g_i}}{p_{g_{i,o}}}-1+\ln\left(\frac{p_{g_{i,o}}}{p_{g_i}}\right)\right)\right]}{1+\frac{1}{2q+1}\frac{fL}{D}}\right\}} \tag{29}$$

where f is given by Eq. (14). As mentioned earlier, the maximum eruption velocity cannot exceed the sound speed given by Eq. (9).

4. Applications

4.1. Test 1: Controlled degassing of Lake Nyos in February 2001

The lakes Nyos and Monoun contain two main gases, namely CO_2 and CH_4. Because the volume proportion of CH_4 is significant only in Lake Monoun, the Lake Nyos test case considered the CO_2 gas only, while as the Lake Monoun test case considered the simultaneous exsolution of CO_2 and CH_4.

The degassing of Lake Nyos considered in this test case occurred on February 2001. According to Zhang and Kling (2006), the total gas pressure (absolute) in Lake Nyos at 206 m depth, before controlled degassing began in 2001, was 1.54 MPa. Also, according to these authors, the pressure at the surface of Lake Nyos was 0.088 MPa, and the bottom water temperature at Lake Nyos was about 25.2 °C (298.35 K). The water density and kinematic viscosity for this temperature are 996.53 kg/m^3 and 8.6745×10^{-7} m^2/s, respectively, which were obtained from `http://www.mhtl.uwaterloo.ca/old/onlinetools/airprop/airprop.html`. Halbwachs et al. (2004) reported an eruption height of about 50 m in this degassing operation. For the degassing, a 203 m long high-density polyethylene (HDPE) pipe with an inner diameter of 140 mm was used. The Ostwald solubility coefficient for CO_2 gas in water at a temperature of 25.2°C is 0.754, which was obtained from Table 1 using spline interpolation.

In the previous sections, the maximum eruption velocity for smooth and rough pipes was derived. To determine which equation to use, first the equivalent roughness (ϵ) for HDPE pipe is obtained from Pipeflow (2015). According to this reference, for an HDPE pipe, $\epsilon = 0.0015$ mm, which gives a relative roughness (ϵ/D) of 0.0000107. This is a very low relative roughness as $\epsilon/D = 0.00001$ is the lowest value of ϵ/D used in the Moody Chart of Munson et al. (2013) (page 430). Notice in this Moody chart that for $\epsilon/D = 0.00001$, the pipe is smooth for Reynolds number (Re) smaller than about 10^7. In our case studies, the flow velocity doesn't exceed 80 m/s, which gives a maximum Re of about 10^7. Thus, the pipe in this case study is smooth and Equation (20) is used to estimate the maximum eruption velocity. To estimate L in Equation (20), note that for the occurrence of degassing, the pump needs to raise the water from the bottom of the lake up to a level where it becomes saturated with gas (i.e., the dissolved gas pressure needs to exceed the local hydrostatic pressure). Thus, the maximum length of eruption column (L) in Eq. (20) can be determined as (1.54 - 0.088)x10^6/(9.8x996.53), which gives 148.7 m. The

actual length L was not reported. Figures (4) and (5) show the calculated and "observed" eruption velocities and heights, respectively, for L values between 140 and 150 m. The "observed" eruption velocity was calculated using the ballistic equation ($w = \sqrt{2gH}$), which assumes perfect conversion of kinetic energy to potential energy. Karlstrom et al. (2013) utilized the ballistic equation along particle image velocimetry (PIV) to estimate the eruption velocity at Lone Star geyser in Yellowstone National Park, USA. Comparison of these methods suggested that in liquid dominated eruptions, PIV and ballistic methods provide upper and lower bounds for the eruption velocity, respectively. Only when the eruption was steam dominated, the ballistic equation overestimated the eruption velocity. The present paper focuses on lake eruptions (cold geysers) which are due to gas exsolution and hence the eruptions are gas dominated. Thus, it would be expected that the ballistic equation overestimates slightly the eruption velocity. In the present test case, the reported eruption height was about 50 m, which gives an eruption velocity of 31.3 m/s.

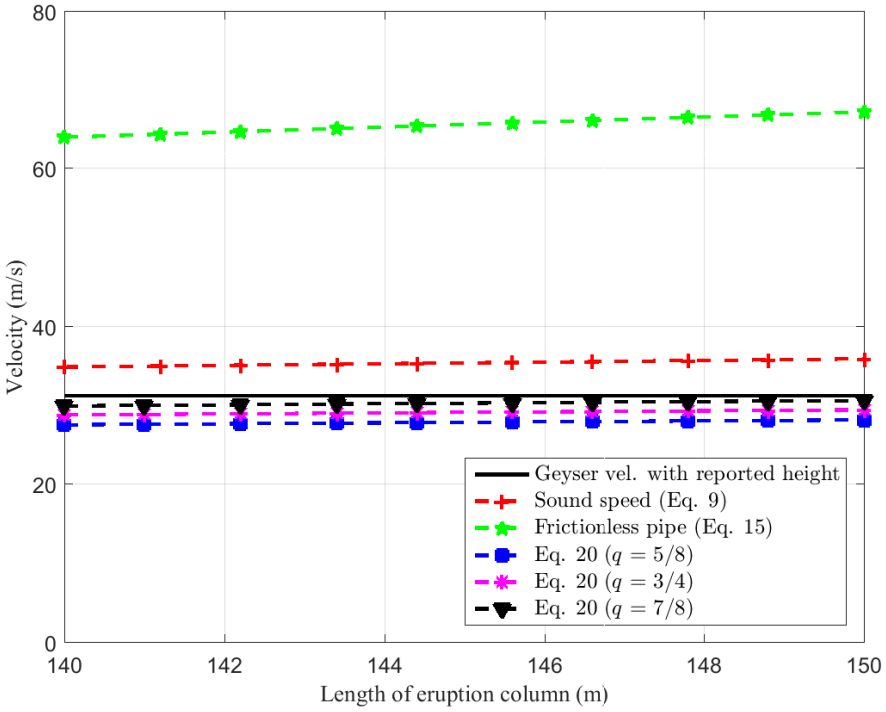

Figure 4. Calculated and "observed" eruption velocities for the controlled degassing operation of Lake Nyos in February 2001

As can be observed in Figures (4) and (5), the calculated eruption heights and velocities using Eqs. (9) and (20) agree well with the corresponding reported values. It is expected that degassing will start as soon as the gas pressure exceeds

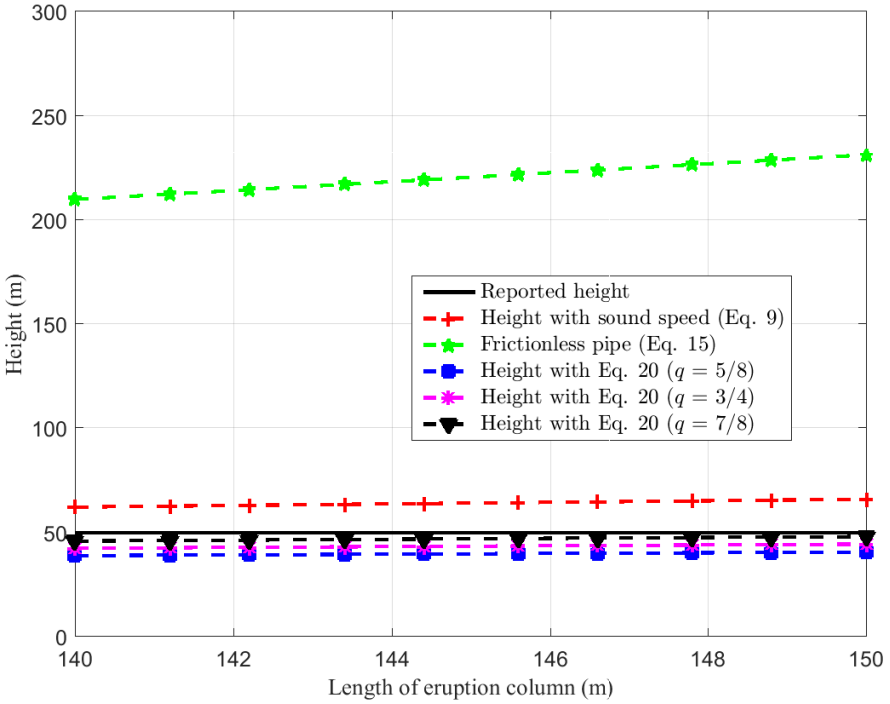

Figure 5. Calculated and "observed" eruption heights for the controlled degassing operation of Lake Nyos in February 2001

the local hydrostatic pressure, thus the actual value of L should be very close to the maximum L (148.7 m). From the results above (Figs. 4 and 5), it appears that Eq. (9) overestimates the eruption height and velocity. Eq. (20) gives lower heights and velocities than Eq. (9) and is in closer agreement with the reported values, especially for accelerating columns closer to the maximum L.

4.2. Test 2: Controlled degassing of Lake Monoun in February 2003

This second test case focuses on the degassing of Lake Monoun considering simultaneous exsolution of two gases (CO_2 and CH_4).

For the degassing of Lake Monoun during February of 2003, Halbwachs et al. (2004) reported an eruption height of about 8 m. For this degassing, a 73 m long high-density polyethylene (HDPE) pipe with an inner diameter of 100 mm was used. According to Zhang and Kling (2006), the pressure at the surface of Lake Nyos was 0.088 MPa. Since the author was not able to find pressure data at the surface of Lake Monoun, it was assumed that this value is the same as that of Lake Nyos (0.088 MPa). The water temperature at a depth of 73 m in Lake Monoun was about 23.3°C (298.35 K) (Halbwachs et al. 2004). The Ostwald solubility coefficient for CO_2 gas in water at a temperature of 23.3°C is 0.798, which was obtained from Table 1 using spline interpolation. Likewise, the Ostwald solubility coefficient of CH_4 for $T = 23.3$ °C is 0.031.

As discussed earlier, $\phi \approx 1 - \rho/\rho_l$ and $\rho_l/\rho \approx 1 + V^{gas}/V^{liq}$. The measured gas/water volume ratio (V^{gas}/V^{liq}) was 3.2 (Halbwachs et al. 2004), which gives a ρ/ρ_l value of 0.238, which in turn gives a ϕ value of 0.762. The vertical profiles of measured partial pressures of CO_2 and CH_4 in Lake Monoun during February 2003 are shown in Figure 2 in Halbwachs et al. (2004). This figure shows that the total gas pressure at the pipe inlet (i.e., at a depth of 73 m) was 0.6 MPa, of which 0.44 MPa and 0.16 MPa were the partial pressures of CO_2 and CH_4, respectively. For the occurrence of gas exsolution (degassing), the pump needs to raise the water from the pipe inlet (73 m deep) up to a level where the total gas pressure exceeds the local hydrostatic pressure. Note in Figure 2 in Halbwachs et al. (2004) that the total gas pressure at the pipe inlet will exceed the hydrostatic pressure at a depth of about 53m. Thus, the maximum length of the accelerating mixture (L) will be about 53m. Because degassing will start as soon as the total gas pressure exceeds the local hydrostatic pressure, the actual value of L should be close to 53 m. Because the value of L was not reported, the eruption height and velocity are calculated for various values of L close to its maximum (53 m). The distribution of partial pressures at $z = 0$ is assumed to be the same as that of a depth of 73 m, which means that the partial pressure of CO_2 at $z = 0$ is $0.733p_o$ ($0.44/0.60\ p_o$) and that of CH_4 is $0.267p_o$ ($0.16/0.60\ p_o$).

In a similar manner to Test 1, it can be shown that the pipe for the second test case is smooth and hence, Eq. (28) is used to estimate the maximum eruption velocity. To utilize Eq. (28), the values of the partial pressures of CO_2 and CH_4 at the water surface (at eruption) are needed, which are determined using Eqs. (25) and (26).

For comparison, the eruption height and velocity when considering a single gas (CO_2) are also calculated using Eq. (20) with $q = 3/4$. This calculation assumes that the total gas pressure is only due to CO_2. Figures (6) and (7) show the calculated and "observed" eruption velocities and heights for L values slightly smaller than 53 m.

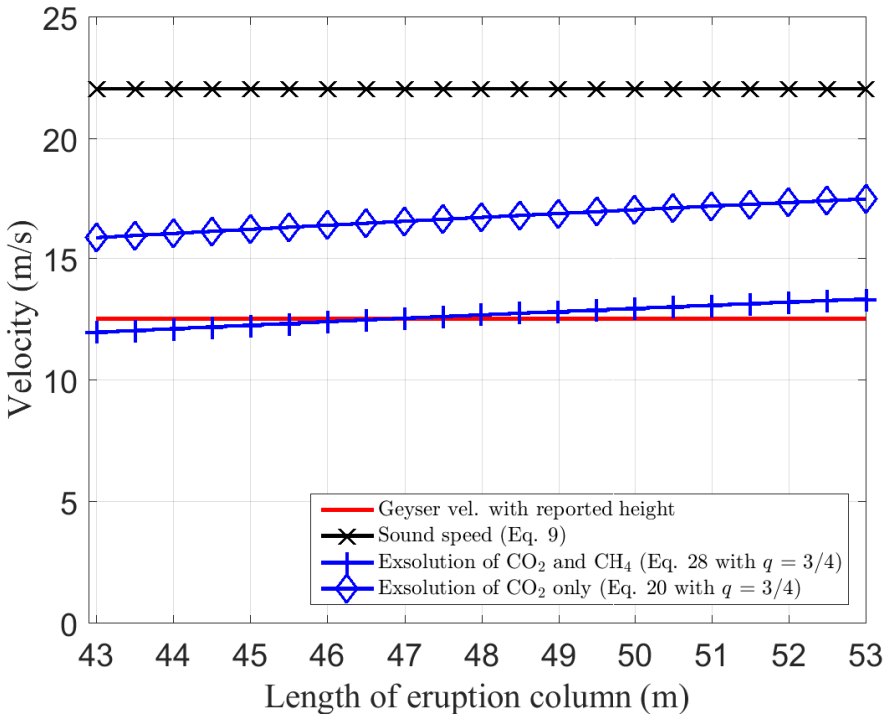

Figure 6. Calculated and "observed" eruption velocities for the controlled degassing operation of Lake Monoun in February 2003

As can be observed in Figs. (6) and (7), the calculated eruption heights and velocities considering the two main gases measured in this lake (CO_2 and CH_4) have a better agreement with the measurements compared to that obtained considering the main gas only (CO_2) and that based on the sound speed. As expected, the eruption height and velocity based on the sound speed give the highest values as the sound speed is the maximum velocity that an eruption can attain. The results also show that the eruption intensity increases with the length of accelerating water column in the vertical pipe.

5. Conclusions

This paper describes two new mathematical models for predicting eruption velocity in degassing pipes based on exsolution of a single gas and the simulta-

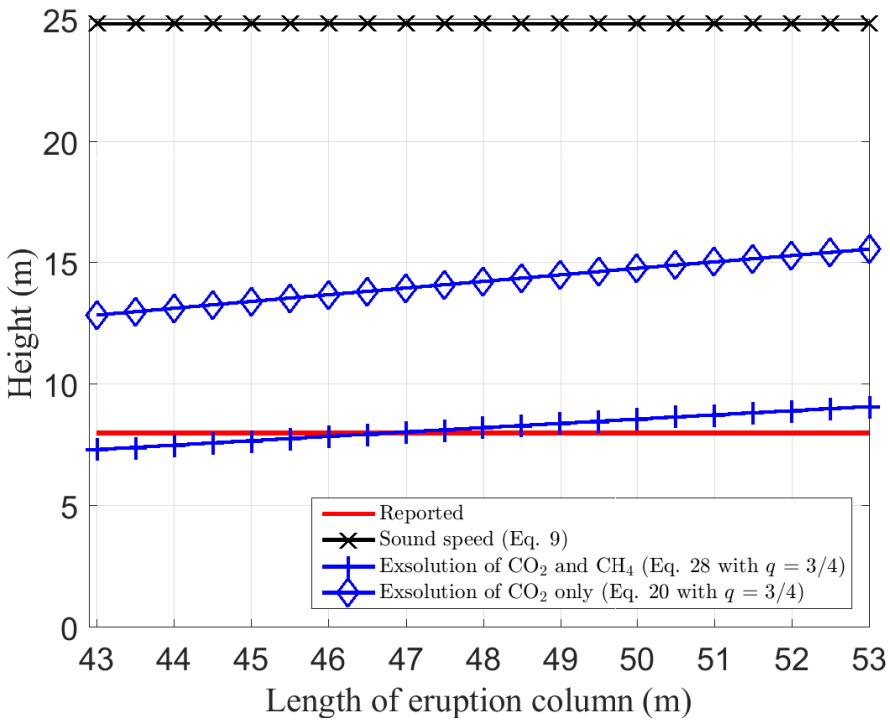

Figure 7. Calculated and "observed" eruption heights for the controlled degassing operation of Lake Monoun in February 2003

neous exsolution of multiple gases. The models were applied to the degassing system of lakes Nyos and Monoun, which contain two main gases, namely CO_2 and CH_4. Because the volume proportion of CH_4 is significant only in Lake Monoun, the Lake Nyos test case considered the exsolution of CO_2 only, while as the Lake Monoun test case considered the simultaneous exsolution of CO_2 and CH_4. The key results are as follows:

1. The proposed models were found to reproduce with good approximation the observed data in both test cases.
2. The results of the model for the eruption in Lake Monoun (Test 2) considering the two main gases measured in this lake (CO_2 and CH_4) were found to have a better agreement with the measurements compared to the model results obtained considering the main gas only (CO_2).
3. When considering exsolution of a single gas, the intensity of the eruption is proportional to the solubility coefficient (solubility at a specific pressure) according to Eqs. (20) and (21). The higher the solubility coefficient, the larger is the eruption intensity.
4. When considering simultaneous exsolution of multiple gases, according to Eqs. (28) and (29), the eruption intensity is proportional to $\sum_{i=1}^{n} \lambda_i p_{g_{i,o}}$, which is the product of the solubility coefficients and their respective partial pressures (or gas concentrations).
5. The results for both tests showed that eruption intensity increases with the length of accelerating water column in the vertical pipe.

Overall, the exsolution of a dissolved gas or dissolved gases can propel large eruption heights and velocities.

Acknowledgments

The author gratefully acknowledges the financial support of the U.S. Environmental Protection Agency under Grant number R835187. The author is also grateful to Prof. Youxue Zhang from the University of Michigan for his help in the derivation of Eq. 16. The author is also very grateful to the Editor and an anonymous reviewer for their constructive comments, which greatly improved the quality of the manuscript. This manuscript has not been formally reviewed by EPA. The views expressed are solely those of the authors. EPA does not endorse any products or commercial services mentioned.

Appendix A

In this appendix, Eqs. (22) and (23) are derived. At any elevation z, the total mass (m_t) is equal to the sum of liquid mass (m^{liq}) and gas mass (m^{gas}), which can be written as

$$\rho(V^{liq} + V^{gas}) = \rho_l V^{liq} + m^{gas} \tag{30}$$

where V is volume (e.g., in m^3) and the superscript indicates the phase (gas or liquid). Because the total mass of gas (m^{gas}) is much smaller than the mass of liquid ($\rho_l V^{liq}$), m^{gas} can be neglected. Hence, Eq. (30) can be approximated as

$$\frac{\rho_l}{\rho} \approx 1 + \frac{V^{gas}}{V^{liq}} \tag{31}$$

Following, let's consider equilibrium exsolution of gases, where the gas phase is not lost from the system. The mass conservation for gas component 1 leads to:

$$C_{g1,o}^{liq} V_o^{liq} = C_{g1}^{liq} V^{liq} + C_{g1}^{gas} V^{gas} \tag{32}$$

where C is concentration (e.g., in kg/m^3), the subscript g_1 indicates gas component 1, and the subscript o indicates the initial state ($z = 0$), which is assumed to be at the pressure of saturation (no gas phase was present initially).

Approximating $V^{liq} \approx V_o^{liq}$, we obtain

$$C_{g1,o}^{liq} \approx C_{g1}^{liq} + C_{g1}^{gas} \frac{V^{gas}}{V_o^{liq}} \tag{33}$$

Eq. (33) can be rewritten as

$$\frac{V^{gas}}{V_o^{liq}} \approx \frac{C_{g1,o}^{liq} - C_{g1}^{liq}}{C_{g1}^{gas}} \tag{34}$$

By definition of the Ostwald solubility coefficient (λ)

$$\lambda_i = \frac{C_{gi}^{liq}}{C_{gi}^{gas}} \tag{35}$$

Substituting Eq. (35) into Eq. (34), gives

$$\frac{V^{gas}}{V_o^{liq}} \approx \frac{C_{g1,o}^{liq}}{C_{g1}^{gas}} - \lambda_1 \tag{36}$$

Similarly, for gas i

$$\frac{V^{gas}}{V_o^{liq}} \approx \frac{C_{gi,o}^{liq}}{C_{gi}^{gas}} - \lambda_i \tag{37}$$

Therefore, from Eq. (36) and Eq. (37)

$$\frac{C_{g1,o}^{liq}}{C_{g1}^{gas}} - \lambda_1 \approx \frac{C_{gi,o}^{liq}}{C_{gi}^{gas}} - \lambda_i \ \forall i \text{ from 2 to } n \tag{38}$$

Using the equation of state of gas i,

$$C_{gi}^{gas} = \frac{P_{gi}}{R_{gi} T} \ \forall i \text{ from 1 to } n \tag{39}$$

where R_g is gas constant in $\mathrm{Jkg^{-1}K^{-1}}$ ($188.9\ \mathrm{Jkg^{-1}K^{-1}}$ for CO_2). Combining the equation of state of gas i and Eq. (35) gives

$$C_{g_{i,o}}^{liq} = \lambda_i \frac{P_{g_{i,o}}}{R_{g_i} T_o} \ \forall i \text{ from 1 to } n \tag{40}$$

Assuming again isothermal conditions ($T = T_o$), and substituting Eqs. (39) and (40) into Eq. (37), the following equation is obtained

$$\frac{V^{gas}}{V_o^{liq}} \approx \frac{\lambda_i p_{g_{i,o}}}{p_{g_i}} - \lambda_i \tag{41}$$

Substituting Eq. (41) into Eq. (31) gives

$$\frac{\rho_l}{\rho} \approx 1 + \lambda_i \frac{p_{g_{i,o}} - p_{g_i}}{p_{g_i}} \tag{42}$$

which is Eq. (22).

Substituting Eqs. (39) and (40) into Eq. (38) gives

$$\frac{\lambda_1 p_{g_{1,o}}}{p_{g_1}} - \lambda_1 = \frac{\lambda_i p_{g_{i,o}}}{p_{g_i}} - \lambda_i \ \forall i \text{ from 2 to } n \tag{43}$$

which is Eq. (23).

Appendix B

In this appendix, Eq. (27) is derived. Using Eq. (22) and noting that $dp = \sum_{i=1}^{n} dp_{g_i}$, $\int (1/\rho) dp$ can be expanded as follows:

$$\int \frac{1}{\rho} dp = \frac{1}{\rho_l} \left[\int_{p_{g_{1,o}}}^{p_{g_1}} \left(1 + \lambda_1 \frac{p_{g_{1,o}} - p_{g_1}}{p_{g_1}} \right) dp_{g_1} + \int_{p_{g_{2,o}}}^{p_{g_2}} \left(1 + \lambda_2 \frac{p_{g_{2,o}} - p_{g_2}}{p_{g_2}} \right) dp_{g_2} + \ldots \right] \tag{44}$$

Noting that $\sum_{i=1}^{n} p_{g_i} = p_{atm}$ and $\sum_{i=1}^{n} p_{g_{i,o}} = p_o$, the evaluation of the integrals in Eq. (44) gives

$$\int \frac{1}{\rho} dp = \frac{1}{\rho_l} (p_{atm} - p_o) + \frac{1}{\rho_l} \sum_{i=1}^{n} \left[\lambda_i p_{g_{i,o}} \left(1 - \frac{p_{g_i}}{p_{g_{i,o}}} - \ln \left(\frac{p_{g_{i,o}}}{p_{g_i}} \right) \right) \right] \tag{45}$$

Assuming that the exsolution of gases is assumed to initiate at hydrostatic pressure (e.g., $p_o = p_{\mathrm{atm}} + \rho g L$), Eq. (45) can be reduced to

$$\int \frac{1}{\rho} dp = -gL + \frac{1}{\rho_l} \sum_{i=1}^{n} \left[\lambda_i p_{g_{i,o}} \left(1 - \frac{p_{g_i}}{p_{g_{i,o}}} - \ln \left(\frac{p_{g_{i,o}}}{p_{g_i}} \right) \right) \right] \tag{46}$$

which is Eq. (27).

References

Atomistry, 2015. Solubility of gases in water. URL: http://oxygen.atomistry.com/solubility_of_gases_in_water.html.

Halbwachs, M., Sabroux, J.C., Grangeon, J., Kayser, G., Tochon-Danguy, J.C., 2004. Degassing the killer lakes Nyos and Monoun, Cameroon. Eos 85, 281.

Hutter, G.M., 1993. Reference data sheet on sewer gas(es). URL: http://www.meridianeng.com/Reference%20Data%20Sheet%20on%20Sewer%20Gases.pdf.

Issa, Ohba, T., Tchamabe, B.C., Padron, E., Hernandez, P., Takem, E.E., Barrancos, J., Sighomnoun, D., Ooki, S., Nkamdjou, S., Kusakabe, M., Yoshida, Y., Dionis, S., 2014. Gas emission from diffuse degassing structures (DDS) of the Cameroon volcanic line (CVL): Implications for the prevention of CO_2-related hazards. Journal of Volcanology and Geothermal Research 283, 82 – 93.

Joseph, D.D., Yang, B.H., 2010. Friction factor correlations for laminar, transition and turbulent flow in smooth pipes. Physica D: Nonlinear Phenomena 239, 1318 – 1328.

Karlstrom, L., Hurwitz, S., Sohn, R., Vandemeulebrouck, J., Murphy, F., Rudolph, M.L., Johnston, M.J.S., Manga, M., McCleskey, R.B., 2013. Eruptions at lone star geyser, yellowstone national park, usa: 1. energetics and eruption dynamics. Journal of Geophysical Research: Solid Earth 118, 4048–4062. doi:10.1002/jgrb.50251.

Kim, H., Kim, K., Song, E., Song, J., 2015. Measurement of friction factor of nickel foam anode at high temperature condition of carbonate flow in direct coal fuel cell system. Applied Thermal Engineering 89, 600 – 608.

Kling, G., Evans, W., Tanyileke, G., Kusakabe, M., Ohba, T., 2005. Degassing lakes Nyos and Monoun: defusing certain disaster. Proc. Natl. Acad. Sci. USA 102, 14185.

Kusakabe, M., Tanyileke, G., McCord, S., Schladow, S., 2000. Recent pH and CO_2 profiles at Lakes Nyos and Monoun, Cameroon: implications for the degassing strategy and its numerical simulation. Journal of Volcanology and Geothermal Research 97, 241 – 260.

Ledig, P.G., 1924. Absorption of carbon dioxide and ammonia from gas bubbles. Industrial & Engineering Chemistry 16, 1231–1233.

Mastin, L.G., 1995. A numerical program for steady-state flow of hawaiian magma-gas mixtures through vertical eruption conduits. U. S. Geol. Surv. Open-File Rep. , 95.

McKeon, B.J., Swanson, C.J., Zagarola, M.V., Donnelly, R.J., Smits, A.J., 2004. Friction factors for smooth pipe flow. Journal of Fluid Mechanics 511, 41–44. doi:10.1017/S0022112004009796.

Munson, B.R., Okiishi, T.H., Huebsch, W.W., Rothmayer, A.P., 2013. Fundamentals of Fluid Mechanics, 7th Edition. John Wiley and Sons, Inc.

Pipeflow, 2015. Pipe roughness. URL: http://www.pipeflow.com/sitemap/pipe-roughness.

Schlichting, H., 1979. Boundary-Layer Theory, 7th edn (translated from the German by J Kestin). McGraw-Hill, New York.

Shapiro, A., 1954. The Dynamics and Thermodynamics of Compressible Fluid Flow, Volume II. The Ronald Press Company, New York.

Sigurdsson, H., Devine, J., Tchua, F., Presser, F., Pringle, M., Evans, W., 1987. Origin of the lethal gas burst from lake monoun, cameroun. Journal of Volcanology and Geothermal Research 31, 1 – 16.

Viana, P., Yin, K., Zhao, X., Rockne, K., 2007. Modeling and control of gas ebullition in capped sediments, in: Proceedings of the 4th International Conference on Remediation of Contaminated Sediments, Battelle Press, Columbus, OH, USA. pp. 22–25.

Weast, R.C., 1984. Handbook of Chemistry and Physics, 64th Edition. CRC Press.

Wilson, L., Sparks, R., Walker, G., 1980. Explosive volcanic eruptions - iv. the control of magma properties and conduit geometry on eruption column behavior. Geophys. J. R. Astron. Soc. 63, 117–148.

Woods, A.W., 1995. The dynamics of explosive volcanic eruptions. Rev. Geophys. 33, 495.

Zhang, Y., 1996. Dynamics of CO_2-driven lake eruptions. Nature 379, 57.

Zhang, Y., 1997. Dynamics of gas-driven eruptions: experimental simulations using CO_2-H_2O-polymer system. J. Geophys. Res. 102, 3077–3096.

Zhang, Y., 1998. Experimental simulations of gas-driven eruptions: kinetics of bubble growth and effect of geometry. Bull. Volcanol. 59, 281–290.

Zhang, Y., 2000. Energetics of gas-driven limnic and volcanic eruptions. J. Volcanol. Geotherm. Res. 97, 215.

Zhang, Y., Kling, G.W., 2006. Dynamics of lake eruptions and possible ocean eruptions. Annual Review of Earth and Planetary Sciences 34, 293–324.